Histol Histopathol (2024) 39: 747-760

Histology and Histopathology
From Cell Biology to Tissue Engineering

ORIGINAL ARTICLE Open Access

ZKSCAN5 activates LAPTM5 expression by recruiting SETD7 to promote metastasis in pancreatic ductal adenocarcinoma

Yong Yang[1,2*], Wei Xie[3*], Xuan Qiao[4], Jun Yang[2], Dan Yao[5] and Dongming Zhu[1]

[1]Department of General Surgery, The First Affiliated Hospital of Soochow University, Suzhou, [2]Department of Hepatobiliary and Pancreatic Surgery, the Affiliated Hospital of Xuzhou Medical University, Xuzhou, [3]Department of General Surgery, Jurong Hospital Affiliated to Jiangsu University, Zhenjiang, [4]Graduate School, Xuzhou Medical University, Xuzhou and [5]Department of Gastrointestinal Surgery, Huai'an Second People's Hospital, the Affiliated Huai'an Hospital of Xuzhou Medical University, Huai'an, Jiangsu, PR China

*Yong Yang and Wei Xie contributed equally to this work

Summary. Lysosomal-associated transmembrane protein 5 (LAPTM5) has been associated with poor prognosis in cancer patients. Its role in regulating metastasis in pancreatic ductal adenocarcinoma (PDAC), however, remains vague. The study here aimed to expound the metastasis-promoting properties of LAPTM5 in PDAC and the detailed mechanism. LAPTM5 was overexpressed in metastatic PDAC cells and was related to the dismal prognosis of patients in GEO datasets. By using lentiviral vectors harboring short hairpin RNA, we found that LAPTM5 downregulation reduced PDAC cell viability, proliferation, and aggressiveness *in vitro* and liver metastasis *in vivo*. Zinc finger with KRAB and SCAN domains 5 (ZKSCAN5) was predicted and verified to mediate LAPTM5 transcription in PDAC cells. Both ZKSCAN5 and SET domains, containing lysine methyltransferase 7 (SETD7) bound to the LAPTM5 promoter, and ZKSCAN5 recruited SETD7 to form a complex promoting LAPTM5 transcription. LAPTM5 knockdown reversed the promoting effect of ZKSCAN5 on the metastasis of PDAC cells. Thus, our findings on the ZKSCAN5/SETD7/LAPTM5 axis provide insights into the underlying mechanism of liver metastasis dissemination in PDAC.

Key words: LAPTM5, ZKSCAN5, Pancreatic ductal adenocarcinoma, SETD7, Liver metastasis

Corresponding Author: Dongming Zhu, Department of General Surgery, The First Affiliated Hospital of Soochow University, No. 188, Shizi Street, Gusu District, Suzhou 215000, Jiangsu, PR China. e-mail: Zhudm_gs913@163.com

www.hh.um.es. DOI: 10.14670/HH-18-678

Introduction

Pancreatic cancer is related to an extremely poor prognosis and high mortality since it is usually diagnosed at advanced stages with metastasized tumor cells (Ren et al., 2018), and liver metastases are commonly detected in a range of malignancies, including pancreatic cancer (Tsilimigras et al., 2021). Pancreatic ductal adenocarcinoma (PDAC) represents about 95% of all pancreatic cancer cases, and the current front-line treatment in local stages comprises surgical resection and adjuvant chemotherapy (De Dosso et al., 2021). However, these treatment modalities have been shown to have limited effectiveness in patients with metastatic PDAC, and multimodality treatment (chemotherapy, radiation therapy, and/or herbal medicine) is well tolerated by patients with pancreatic cancer and liver metastases and may be effective in prolonging their survival (Ouyang et al., 2011; Gasmi et al., 2021; Zafar et al., 2023). Still, effective therapeutic strategies are lacking. Hence, it is urgent to explore promising therapy strategies for patients with PDAC.

In the present study, two datasets, GSE144909 (the gene expression differences between pancreatic cancer cell lines and its high liver metastatic lines) and GSE19281 (primary PDAC samples and liver metastasis samples), were queried and intersected in an attempt to decipher genes that are related to liver metastasis in PDAC. Four candidates were screened out: lysosomal-associated transmembrane protein 5 (LAPTM5), ERG, LMO2, and follistatin-related protein 1 (FSTL1). Our preliminary bioinformatics prediction suggested that only LAPTM5, LMO2, and FSTL1 showed prognostic value in PDAC. Meanwhile, the role of LMO2 (Nakata et al., 2009) and FSTL1 (Viloria et al., 2016) have been

studied in the context of pancreatic cancer. Even though LAPTM5 was identified as a key candidate that could be used as a prognostic biomarker and potential therapeutic target for kidney renal clear cell carcinoma (Sui et al., 2021), its functional role in PDAC has not been clarified. Intriguingly, LAPTM5 has been reported to be directly activated by the transcription factor runt-related transcription factor 2 in osteoblastic cells (Geng et al., 2019). By query in the UCSC Genome Browser (https://genome.ucsc.edu/index.html) website, we found two transcription factors that share binding sites near the LAPTM5 promoter: Zinc finger with KRAB and SCAN domains 5 (ZKSCAN5) and EWSR1-FLI1. The EWSR1-FLI1 oncogene has been verified to be insufficient to induce the development of pancreatic cancer (Fahr et al., 2020). Meanwhile, ZKSCAN5 has been recently verified to activate the transcription of vascular endothelial growth factor C by recruiting SET domains containing lysine methyltransferase 7 (SETD7) to promote the metastasis of breast cancer (Li et al., 2022). SETD7 also termed KIAA1717, KMT7, or SET7/9, was identified as a histone H3-lysine 4-specific (H3K4) methyltransferase that governs the affinity between histone 3 and double-stranded DNA to modulate gene expression (Chiang et al., 2022). Therefore, our study here was to characterize the pro-metastatic role of LAPTM5 in PDAC and to elucidate the mechanism concerning ZKSCAN5/SETD7.

Materials and methods

Bioinformatics

The Gene Expression Omnibus (GEO) repository (https://www.ncbi.nlm.nih.gov/gds/?term=) was used to analyze potential molecular mechanisms leading to liver metastasis in PDAC. Wild-type cell samples (GSM4300586 and GSM4300588) and high liver metastatic cell samples (GSM4300587 and GSM4300589) from the GSE144909 dataset, as well as primary PDAC (GSM478458~GSM478461) and liver metastasis (GSM478465~GSM478469) in the GSE19281 dataset were used. Genes differentially expressed in metastatic PDAC were screened using $p<0.01$ as the significance threshold.

The PDAC cohort (n=177, RNA-seq HTSeq counts and survival data were acquired from the TCGA-PDAC repository) in the Kaplan-Meier Plotter (httP://kmplot.com/analysis) was included to analyze the significance of gene expression in predicting recurrence-free survival (RFS). The GEPIA platform (http://gepia.cancer-pku.cn/detail.php) was used to analyze the correlation between gene expression in tumor tissues of patients with pancreatic adenocarcinoma (derived from TCGA-pancreatic adenocarcinoma RNA-Seq data).

Cell culture and infection

Biopsy xenografts of PDAC line-3 (BxPC-3, CL-0042) and PDAC cell lines derived from metastatic lesions, ASPC-1 (CL-0027), CFPAC-1 (CL-0059), and Capan-1 (CL-0708) cells were purchased from Procell (Wuhan, Hubei, China). All cells were correctly identified by short tandem repeat and the source of the relevant cell lines can be accessed via Cellosaurus - a knowledge resource on cell lines (https://www.cellosaurus.org/index.html). The purchased cells were activated and cultured in Dulbecco's modified Eagle's medium (DMEM) with 10% FBS + 1% P/S (Procell) at 37°C and 5% CO_2.

The ASPC-1 and Capan-1 cells under good growth conditions were seeded into 6-well plates and infected by lentiviral vectors (oe-NC, sh-NC, oe-LAPTM5, oe-ZKSCAN5, sh-LAPTM5, sh-ZKSCAN5, sh-SETD7, oe-ZKSCAN5 + sh-NC, oe-ZKSCAN5 + sh-LAPTM5, oe-ZKSCAN5 + sh-SETD7) when the cell confluence reached about 50%. After 72h of infection, cells were screened with puromycin to obtain stably transfected cells for subsequent experiments. The efficiency of lentiviral intervention on gene expression in stably transfected cells was examined by reverse transcription-quantitative PCR (RT-qPCR).

Cell counting kit-8 (CCK-8) assay for cell viability

ASPC-1 and Capan-1 cells were detached with trypsin and counted after resuspension. The cells were plated in 96-well plates at 2000 cells per well and placed in a 37°C cell incubator. The original CCK8 reagent was diluted to obtain a 10% CCK-8 detector (C0037, Beyotime Biotechnology Co., Ltd., Shanghai, China), which was added to the plate. The 96-well plate was incubated in an incubator for 2h in the dark, and the OD value was measured at 450 nm using a microplate reader.

EdU incorporation assay for cell proliferation

The EdU Assay Kit was used to assess the proliferative activity of the cells (C10310-1, Guangzhou RiboBio Co., Ltd., Guangzhou, Guangdong, China). ASPC-1 and Capan-1 cells (1×10^5 cells/well) were seeded in 96-well plates, and 10 μM EdU detection reagent was supplemented to each well for a 2h incubation. After incubation, 4% paraformaldehyde was added for cell fixation for 30 min, and 0.5% Triton X-100 cell permeabilization solution was used for permeabilization for 10 min after removal of the fixative. The cells were treated with 200 μL Apollo staining solution for 0.5 h at room temperature and with Hoechst 33342 staining solution for 10 min (both in the dark). Immediately after staining was completed, fluorescence microscope photographs were taken for observation, and the proportion of EdU-positive cells was measured using ImageJ software.

Colony formation assay

ASPC-1 and Capan-1 cells were plated at 500

cells/well in 6-well plates and cultured in a medium containing 10% FBS for 2 weeks. The colonies were fixed with 4% paraformaldehyde (Sangon, Shanghai, China) for 15 min and stained with 0.1% crystal violet (Sangon). The plates were imaged under an inverted microscope, and the number of colonies formed was counted.

Transwell assays

Transwell chambers were seeded in a 24-well plate, and 70 μL diluted Matrigel was applied to the upper surface of the membranes in the invasion assay. ASPC-1 or Capan-1 cells (1×10^5 cells) resuspended in serum-free DMEM were added to the apical chamber, and the DMEM containing 10% FBS was added to the basolateral chamber. After incubation for 24h, the cells on the lower surface of the Transwell chamber were fixed using 4% paraformaldehyde and stained using 0.1% crystal violet staining solution. The cells that migrated or invaded the basolateral chamber were counted under the microscope.

Tube formation assay

The prepared Matrigel was added to a 96-well plate, and the Matrigel and DMEM were mixed and incubated in an incubator. After gel formation, the human umbilical vein endothelial cells (HUVECs, EH0155, Yuchunbio, Shanghai, China) were washed with Dulbecco's phosphate-buffered saline (DPBS), and the cells were detached with the appropriate amount of ethylenediaminetetraacetic acid-containing trypsin to make a cell suspension and added into Matrigel-coated 96-well plates. The medium from which ASPC-1 or Capan-1 cells were collected was used as the conditioned medium, which was added to 96-well plates containing HUVEC. After a 12h incubation, the plates were washed with DPBS and observed using an inverted microscope.

Flow cytometry

The Annexin V-fluorescein isothiocyanate (FITC)/propidium iodide (PI) double-staining apoptosis assay kit (P-CA-201, Procell) was used for analyzing ASPC-1 and Capan-1 cell apoptosis. The cells were centrifuged at 300 g for 5 min, gently resuspended, and counted. The cells were resuspended by adding diluted 1× Annexin V Binding Buffer working solution, and 5 μL of Annexin V-FITC and 5 μL of PI staining solution were supplemented to the cell suspension. After 15-20 min in darkness at room temperature, the cells were loaded onto a flow cytometer.

RT-qPCR

The TRIzol™ Plus RNA Purification Kit (12183555, Thermo Fisher Scientific Inc., Waltham, MA, USA) was applied to extract total RNA from BxPC-3, ASPC-1, CFPAC-1, and Capan-1 cells, and the extracted RNA was purified. The concentration and purity of the RNA were detected. Reverse transcription and PCR were performed according to HIScript® Q RT SuperMix for qPCR (R123-01, NanJing Vazyme Biotech Co., Ltd., Nanjing, China) and 2x M5 HIPer SYBR Premix Es Taq (MF787-01, Mei5bio, Beijing, China) instructions. β-actin was chosen as the endogenous reference for calculating the relative expression of target genes with the $2^{-\Delta\Delta Ct}$ method. The primer sequences are listed in Table 1.

Western blot

The cells in Eppendorf tubes were centrifuged at 1000 rpm for 5 min. The precipitates were lysed by adding RIPA supplemented with protease inhibitor (Beyotime) to obtain the total proteins, and the protein concentration was quantified by the BCA method (Beyotime). Equal amounts of protein (20 μg) were separated by 10% SDS-PAGE and transferred to polyvinylidene fluoride membranes. The membrane was sealed with skimmed milk for 2h at room temperature and probed with primary antibodies to LAPTM5 (1:1000, A17995, ABclonal, Wuhan, Hubei, China), ZKSCAN5 (1:1000, SAB1407244, Sigma-Aldrich Chemical Company, St Louis, MO, USA), SETD7 (1:1000, SAB5700275, Sigma-Aldrich), and β-actin (1:1000, ab8226, Abcam, Cambridge, UK) at 4°C overnight. After washing, the membranes were probed with horseradish peroxidase (HRP)-labeled secondary antibody goat anti-mouse IgG (1:1000, GTX213111-01, GeneTex, Inc., Alton Pkwy Irvine, CA, USA) and goat anti-rabbit secondary IgG (1:1000, GTX213110-01,

Table 1. Primers used in reverse transcription-quantitative PCR.

Target	Forward sequence (5'-3')	Reverse sequence (5'-3')
LAPTM5	CTCTCCCAGATGGGCTACCT	GACTACGCCGATCAGTAGGC
ZKSCAN5	TTGCATGCTACTGAAAGTGTCC	CCTGAAGCCTCATGGTACTGG
SETD7	GGCTCCACTCCCAAAGATCC	GGCTCCCAGAGTGCGATTTT
β-actin	ACAGAGCCTCGCCTTTGCC	TGGGGTACTTCAGGGTGAGG

LAPTM5, lysosomal protein transmembrane 5; ZKSCAN5, Zinc finger with KRAB and SCAN domains 5; SETD7, SET domain containing lysin methyltransferase 7.

GeneTex) at room temperature for 2h. ECL luminescent solution was used for development, followed by exposure and imaging. The grayscale values of the bands were calculated using ImageJ software to determine the relative expression of the target proteins (normalized to the internal control β-actin).

Chromatin immunoprecipitation (ChIP)

ChIP assays were performed to analyze the levels of ZKSCAN5, SETD7, and H3K4me2/H3K4me3 modifications on the LAPTM5 promoter using the ChIP kit (ab185913, Abcam) according to the manufacturer's instructions. The cells were first cross-linked in 1% formaldehyde at room temperature for 15 min. Unreacted formaldehyde was quenched with glycine, and DNA was fragmented by ultrasonic fragmentation. Among them, 3% of the total chromatin was selected as Input group without IP, and the remaining chromatin was immunoprecipitated using antibodies to ZKSCAN5 (1:100, Sangon), SETD7 (1:50, 730055, Thermo Fisher), H3K4me2 (1:50, 39079, ProteinTech Group, Chicago, IL, USA), H3K4me3 (1:50, 61379, ProteinTech Group), and an isotype control IgG (1:500, A7028, Beyotime). The DNA fragments pulled down by the antibody complex were eluted and purified. qPCR was conducted to detect the enrichment of the LAPTM5 promoter fragment (chr1: 30757674-30758009), and the results were normalized and compared according to the IgG group. The LAPTM5 promoter primer sequences used for qPCR were forward primer: 5'-CCTCTGAGA CACTGAAGGGG-3' and reverse primer: 5'-CTCCTGGGAATGGCAGAGG-3'.

Dual-luciferase reporter assays

The promoter sequence of LAPTM5 (chr1: 30757674-30758009) was inserted into pL3-Basic (E1751, Promega Corporation, Madison, WI, USA) luciferase reporter vectors using restriction endonucleases according to the manufacturer's protocol. The constructed luciferase reporter vectors were subsequently transfected into ASPC-1 and Capan-1 cells with stable knockdown of ZKSCAN5 using Lipofectamine 2000 (Thermo Fisher). After 48h of incubation, the activities of firefly and Renilla luciferases were assessed using a dual-luciferase reporter assay system (Promega Corporation, Madison, WI, USA), and the relative fluorescence intensity was expressed as the ratio of firefly luciferase to Renilla luciferase activity.

Co-immunoprecipitation (Co-IP) assays

The transfected cells were lysed with cell lysis buffer and the supernatant was discarded after a 0.5h centrifugation. A small amount of lysate was collected as Input, and the remaining lysate was incubated with specific antibodies to ZKSCAN5 (1:100, Sangon) or SETD7 (1:200, 24840-1-AP, ProteinTech Group) overnight and with pretreated protein A agarose beads for 2h (both at 4°C). After the immunoprecipitation reaction, the supernatant was carefully aspirated after a 3,000-rpm centrifugation for 3 min, and the agarose beads were washed with 1 mL of RIPA lysis buffer. Western blot analysis was carried out to quantify the bound protein.

Immunofluorescence staining

The cells were fixed with 4% paraformaldehyde for 20 min, permeabilized with 1% Triton X-100 for 5-10 min, and sealed with 10% goat serum for 0.5h (all at room temperature). The cells were probed with the primary antibodies to ZKSCAN5 (1:500, SAB1407244, Sigma-Aldrich) and SETD7 (1:100, SAB5700275, Sigma-Aldrich) overnight at 4°C. Alexa Fluor 555-labeled donkey anti-mouse secondary antibody (1:200, A0460, Beyotime) and Alexa Fluor 488-labeled goat anti-rabbit secondary antibody (1:200, A0423, Beyotime) were supplemented separately for a 1h incubation at room temperature in the dark. DAPI was added for nuclear staining, and finally, the staining was observed under fluorescence microscopy (ZKSCAN5 was labeled in red and SETD7 in green).

Animal experiments

All procedures of animal studies were conducted under guidelines approved by the Institutional Animal Care and Use Committee of the First Affiliated Hospital of Soochow University. Twenty-four BALB/C female nude mice (6-8 weeks old, weight 18-20 g) were purchased from Beijing Vital River Laboratory Animal Technology Co., Ltd. (Beijing, China).

ASPC-1 cells infected with sh-NC or sh-LAPTM5 were resuspended and subcutaneously injected into the right flank of mice (n=6). The mice were monitored for status (body weight, water intake, excretion and activity, fur gloss) and growth of subcutaneous tumors in the lateral abdomen. When the tumor forms a visible bulge, the length L (mm) and width W (mm) of the tumor were measured twice a week with vernier calipers to calculate the volume of the tumor. After 4 weeks, the mice were euthanized with an overdose of anesthetics on an ultra-clean table to remove the tumors.

Similarly, ASPC-1 cells infected with sh-NC or sh-LAPTM5 were resuspended. After anesthetizing the mice, an oblique incision of about 1.0 cm was made on the left upper abdomen, and 1×10^6 ASPC-1 cells were injected into the spleen. After the injection, the pinprick was compressed with a 75% alcohol cotton ball for 2-3 min, and the wound was sutured. After 28 d, the mice were euthanized with an overdose of anesthetics, and the livers were collected. The number of metastatic tumor nodules infiltrating the surface of the liver can be visually counted with the naked eye. The tissues were

then fixed and embedded.

Immunohistochemistry

Tissue sections of subcutaneous xenograft tumors or metastatic liver tumors from mice in each group (n=6) were sequentially soaked in xylene and ethanol for dewaxing and hydration, and heated with citrate buffer for antigen retrieval. The endogenous peroxidase activity was eliminated using 3% hydrogen peroxide. To block nonspecific binding, 5% FBS was added for a 0.5h incubation. The slides were incubated with antibody to E-cadherin (1:500, ab40772, Abcam), Vimentin (1:500, ab92547, Abcam), Ki67 (1:100, SAB5700770-100UL, Sigma-Aldrich), Cleaved-Caspase3 (1:200, PA5-114687, Thermo Fisher), and CD31 (1:50, ab28364, Abcam) overnight at 4°C and with HRP-labeled goat anti-rabbit secondary antibody (1:1000, GTX213110-01, GeneTex) for 2h. The color was developed with the DAB kit (ab64238, Abcam), and hematoxylin was used for counter-staining. The slides were dehydrated in ethanol, cleared with xylene, sealed with neutral gum, and observed under an inverted microscope.

Quantification and statistical analysis

Statistical analyses for figures were performed using GraphPad Prism software (version 8.0, GraphPad, San Diego, CA, USA). Data are presented as the mean ± SD. All experiments were performed at least three independent times. Significance was evaluated by performing a one-way or two-way analysis of variance (ANOVA) with Dunnett's or Sidak's post hoc test. Differences were regarded as having statistical significance with $p<0.05$.

Results

LAPTM5 in metastatic PDAC cells is closely associated with poor prognosis of PDAC patients

We cross-screened the GEO datasets GSE144909 (Fig. 1A) and GSE19281 (Fig. 1B) and found a total of four intersections in both datasets: LAPTM5, ERG, LMO2, FSTL1 (Fig. 1C). The prognostic significance of these four genes on RFS in PDAC patients was analyzed by Kaplan-Meier Plotter. Higher expression of LMO2 predicted higher RFS in patients (Fig. 1D), while higher expression of FSTL1 (Fig. 1E) and LAPTM5 (Fig. 1F) predicted lower RFS in patients. ERG did not have a significant ($p<0.05$) prognostic significance in PDAC (Fig. 1G). Considering that LMO2 (Nakata et al., 2009) and FSTL1 (Viloria et al., 2016) have been studied in PDAC, we chose LAPTM5 as the following study subject.

Applying RT-qPCR and western blot, it was found that LAPTM5 was more highly expressed in metastatic PDAC cell lines ASPC-1, CFPAC-1, and Capan-1 than in BxPC-3 cells (Fig. 1H,I), which rudimentarily validated the prediction results.

Downregulation of LAPTM5 reverts the malignant phenotype of metastatic PDAC cells

To investigate the effect of LAPTM5 on the metastatic properties of PDAC cells, we infected ASPC-1 and Capan-1 cells (two cell lines with higher LAPTM5 expression) with lentivirus specifically targeting LAPTM5 (sh-LAPTM5 1#, 2#, and 3#). After the validation of knockdown using RT-qPCR, sh-LAPTM5-2# (Fig. 2A) with the best knockdown efficiency was selected for the subsequent analyses.

The results of the EdU incorporation and CCK-8 assays showed that cell viability and proliferation were reduced after the knockdown of LAPTM5 (Fig. 2B,C). It was observed using colony formation assay that downregulation of LAPTM5 inhibited cell colony formation (Fig. 2D). Cell migration and invasion were assessed using Transwell assays, which confirmed that the downregulation of LAPTM5 impeded cell aggressiveness (Fig. 2E,F). Cell apoptosis evaluation using flow cytometry demonstrated that the downregulation of LAPTM5 increased the level of apoptosis (Fig. 2G). Angiogenesis experiments showed that the number of tubes formed by HUVECs cultured with conditioned medium from PDAC cells with sh-LAPTM5 was reduced compared with the conditioned medium from PDAC cells in the sh-NC group (Fig. 2H).

LAPTM5 promotes the growth and metastasis of PDAC cells in vivo

To study the effect of LAPTM5 on tumor growth and metastasis, we injected ASPC-1 cells with sh-NC or sh-LAPTM5 subcutaneously into nude mice to observe tumor formation. A reduced volume of xenograft tumors was formed by ASPC-1 cells in the sh-LAPTM5 group relative to tumors formed by ASPC-1 cells in the sh-NC group (Fig. 3A). Immunohistochemical results showed that the knockdown of LAPTM5 decreased the expression of proliferation marker Ki67 and endothelial marker CD31 in the tumor tissues while increasing the expression of the apoptosis marker Cleaved-Caspase3 (Fig. 3B).

Different groups of PDAC cells were injected through the spleen of nude mice to establish an *in vivo* metastatic tumor model and to compare liver metastasis in nude mice. The metastatic tumor nodules infiltrating the liver surface of mice injected with ASPC-1 silencing of LAPTM5 were significantly reduced, indicating that the knockdown of LAPTM5 significantly inhibited the metastasis of tumor cells (Fig. 3C). Knockdown of LAPTM5 remarkably downregulated Vimentin expression and increased E-cadherin expression in liver-infiltrating metastatic tissues as detected by immunohistochemistry (Fig. 3D).

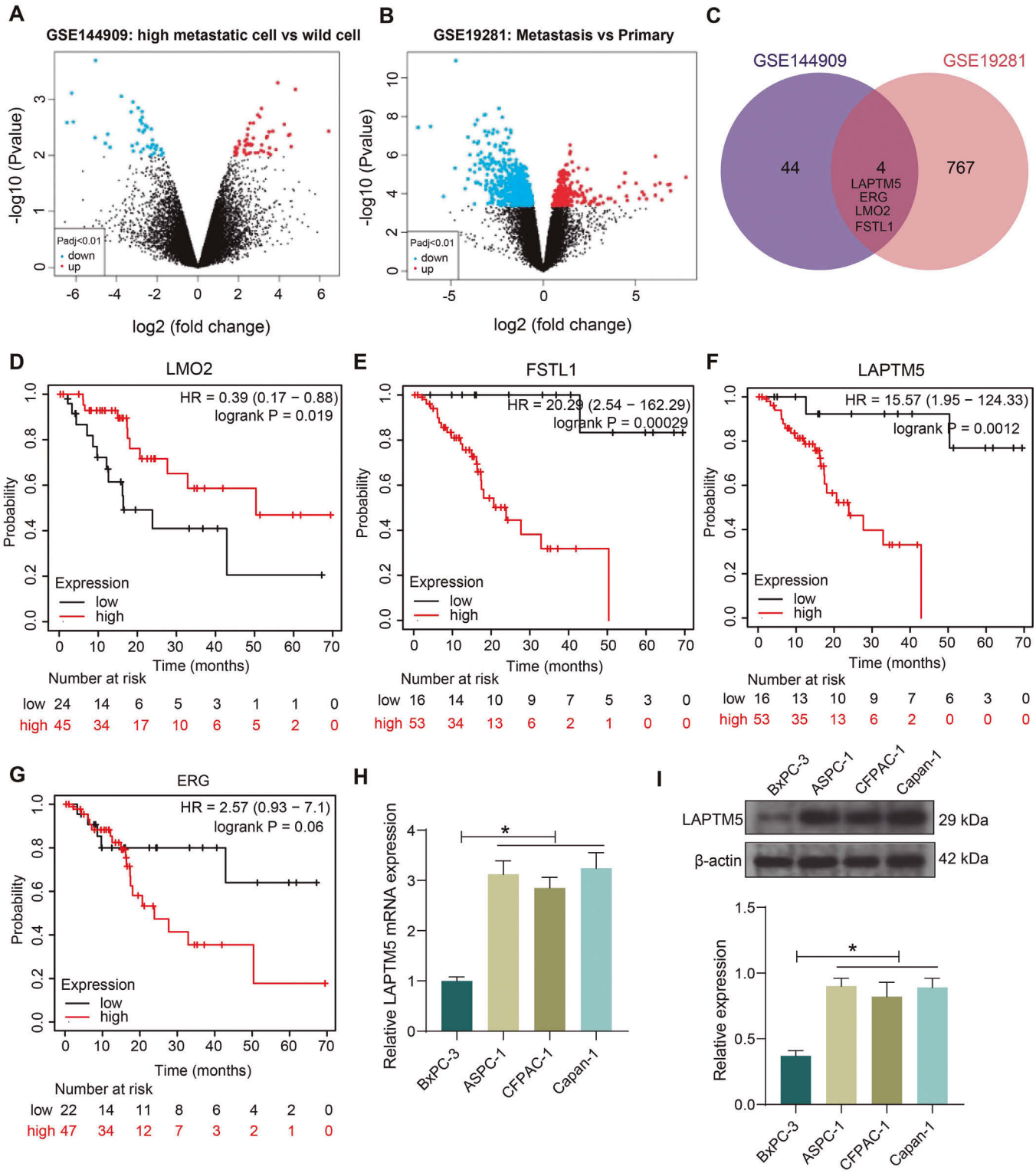

Fig. 1. LAPTM5 is highly expressed in metastatic PDAC *versus* primary tumors and is strongly associated with adverse outcomes in PDAC patients. **A-B.** Volcano maps for the GSE144909 and GSE19281 datasets. **C.** A total of four intersections were found in the two datasets. **D-G.** The prognostic values of LAPTM5, ERG, LMO2, and FSTL1 in predicting RFS of PDAC patients in Kaplan-Meier Plotter (n=177, RNA-seq HTSeq counts and survival data were acquired from the TCGA-PDAC repository). **H.** The mRNA expression of LAPTM5 in BxPC-3 cells and metastatic ASPC-1, CFPAC-1, and Capan-1 cells by RT-qPCR. **I.** The protein expression of LAPTM5 in BxPC-3 cells and metastatic ASPC-1, CFPAC-1, and Capan-1 cells by western blot. Data are presented as the mean ± S.D. n=3. **p*<0.05 by one-way ANOVA.

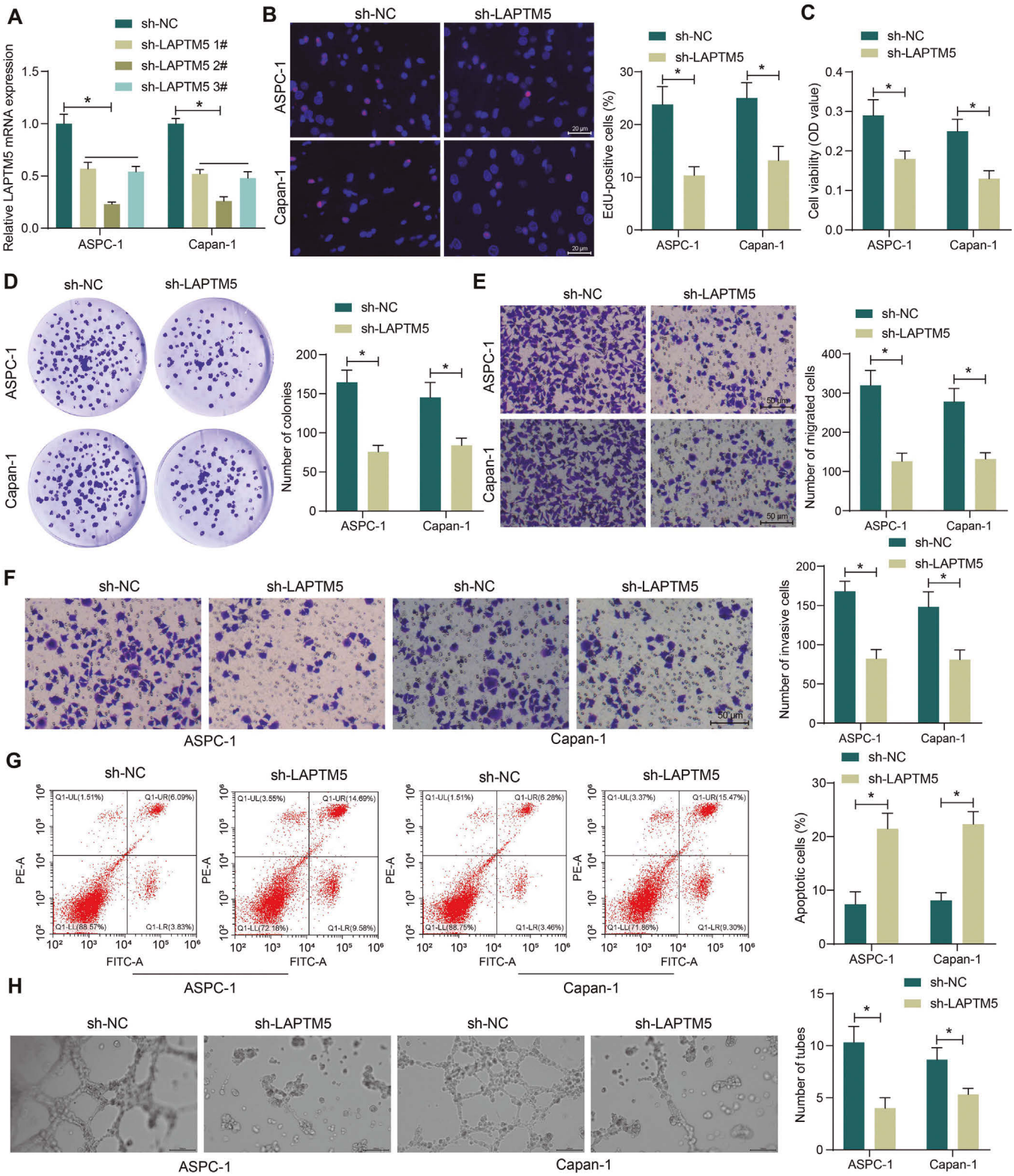

Fig. 2. Downregulation of LAPTM5 inhibits the growth and metastasis of PDAC cells. ASPC-1 and Capan-1 cells were infected with shRNAs targeting LAPTM5 (sh-NC as control). **A.** LAPTM5 expression in ASPC-1 and Capan-1 cells after infection by RT-qPCR. **B.** The proliferation of ASPC-1 and Capan-1 cells by EdU incorporation assay. **C.** The ASPC-1 and Capan-1 cell viability by CCK-8 assay. **D.** Colony forming ability of ASPC-1 and Capan-1 cells by colony formation assays. **E.** The migration ability of ASPC-1 and Capan-1 cells by Transwell migration assay. **F.** The invasion ability of ASPC-1 and Capan-1 cells by Transwell invasion assay. **G.** The apoptosis levels in ASPC-1 and Capan-1 cells by flow cytometry. **H.** The tubes formed by HUVECs cultured with a conditioned medium of PDAC cells with knockdown of LAPTM5 were analyzed using angiogenesis assay. Data are presented as the mean ± S.D. n=3. **p*<0.05 by two-way ANOVA.

ZKSCAN5 mediates the transcription of LAPTM5 in PDAC cells

To analyze the causes of the elevated LAPTM5 expression in metastatic PDAC, we analyzed transcription factors with binding sites near the LAPTM5 promoter using JASPAR on the UCSC Genome Browser (https://genome.ucsc.edu/index.html). The presence of binding sites for ZKSCAN5 and EWSR1-FLI1 was observed near the LAPTM5 promoter (Fig. 4A). The GEPIA database displayed that LAPTM5 expression was significantly positively correlated with

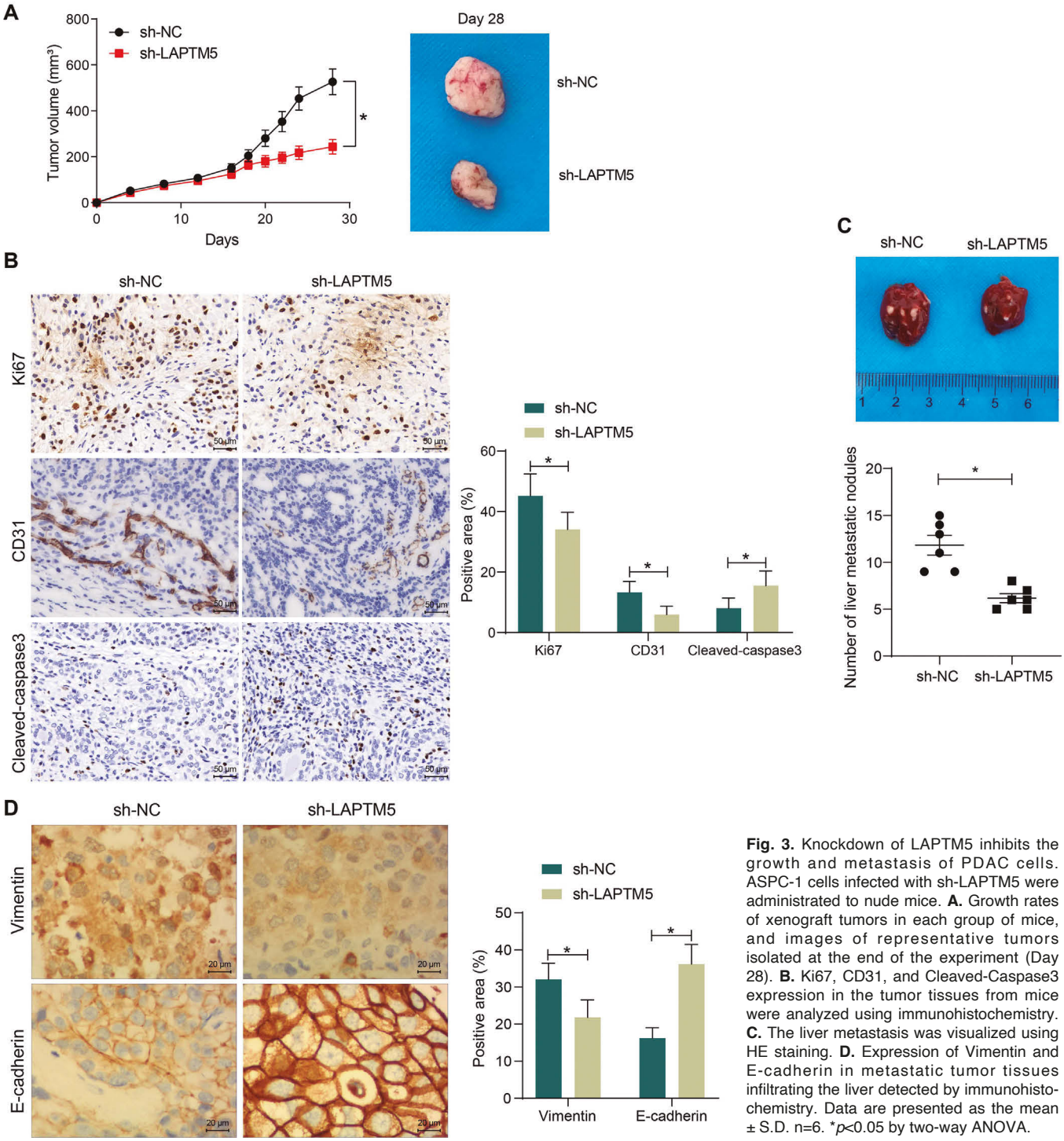

Fig. 3. Knockdown of LAPTM5 inhibits the growth and metastasis of PDAC cells. ASPC-1 cells infected with sh-LAPTM5 were administrated to nude mice. **A.** Growth rates of xenograft tumors in each group of mice, and images of representative tumors isolated at the end of the experiment (Day 28). **B.** Ki67, CD31, and Cleaved-Caspase3 expression in the tumor tissues from mice were analyzed using immunohistochemistry. **C.** The liver metastasis was visualized using HE staining. **D.** Expression of Vimentin and E-cadherin in metastatic tumor tissues infiltrating the liver detected by immunohistochemistry. Data are presented as the mean ± S.D. n=6. *p<0.05 by two-way ANOVA.

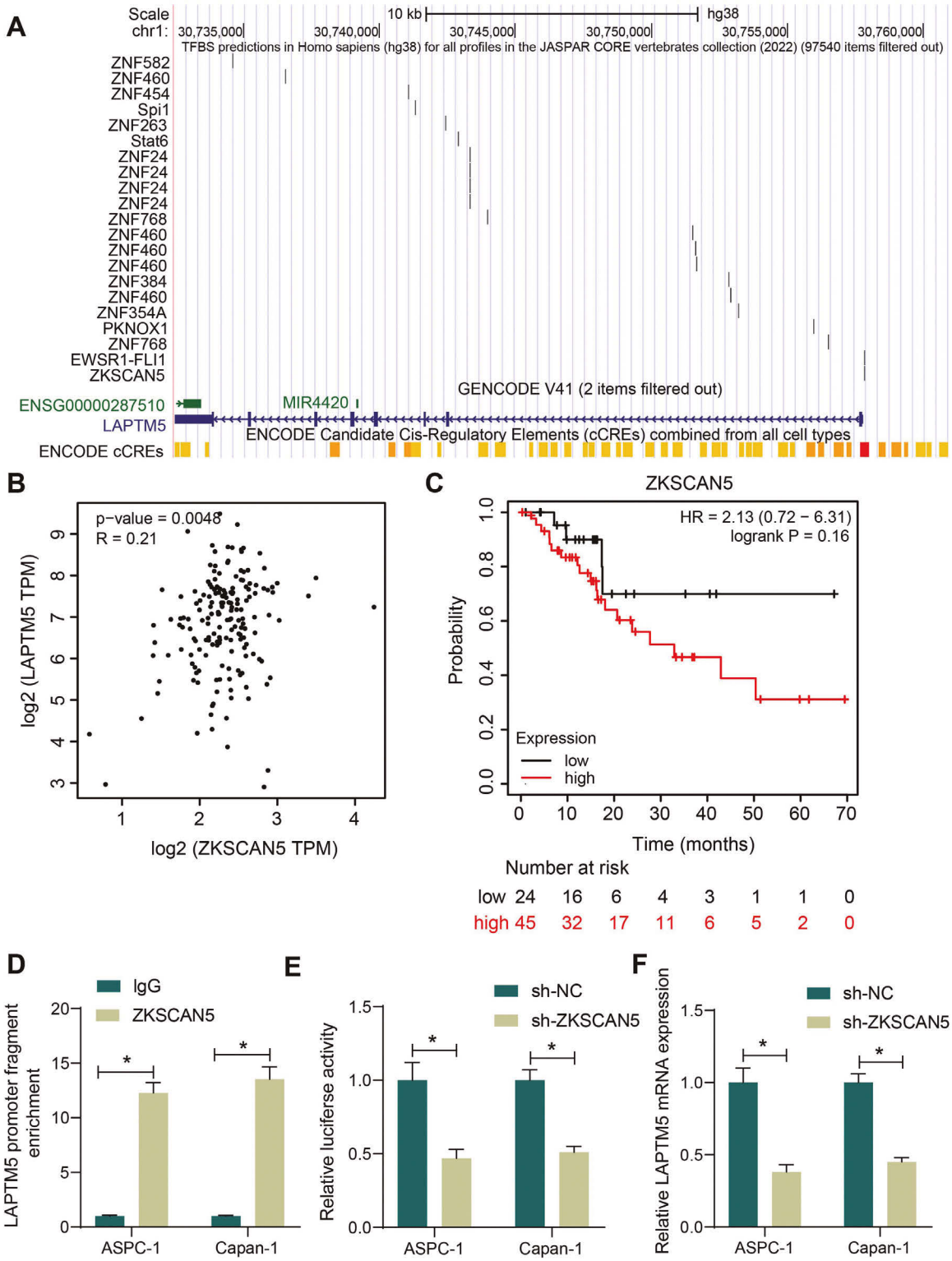

Fig. 4. ZKSCAN5 mediates the transcription of LAPTM5. **A.** JASPAR analysis of transcription factors with binding sites in the vicinity of the LAPTM5 promoter. **B.** GEPIA analysis of the correlation between LAPTM5 and ZKSCAN5 expression in tumor tissues of patients with pancreatic adenocarcinoma (from RNA-Seq data of TCGA-pancreatic adenocarcinoma). **C.** The prognostic value of ZKSCAN5 in predicting RFS of PDAC patients in Kaplan-Meier Plotter (n=177, RNA-seq HTSeq counts and survival data were acquired from the TCGA-PDAC repository). **D.** The enrichment of LAPTM5 promoter by ZKSCAN5 in ASPC-1 and Capan-1 cells by ChIP-qPCR assay. **E.** The effect of ZKSCAN5 knockdown on luciferase activity using a dual-luciferase reporter assay. **F.** LAPTM5 mRNA expression in ASPC-1 and Capan-1 cells with knockdown of ZKSCAN5 using RT-qPCR. Data are presented as the mean ± S.D. n=3. **p*<0.05 by two-way ANOVA.

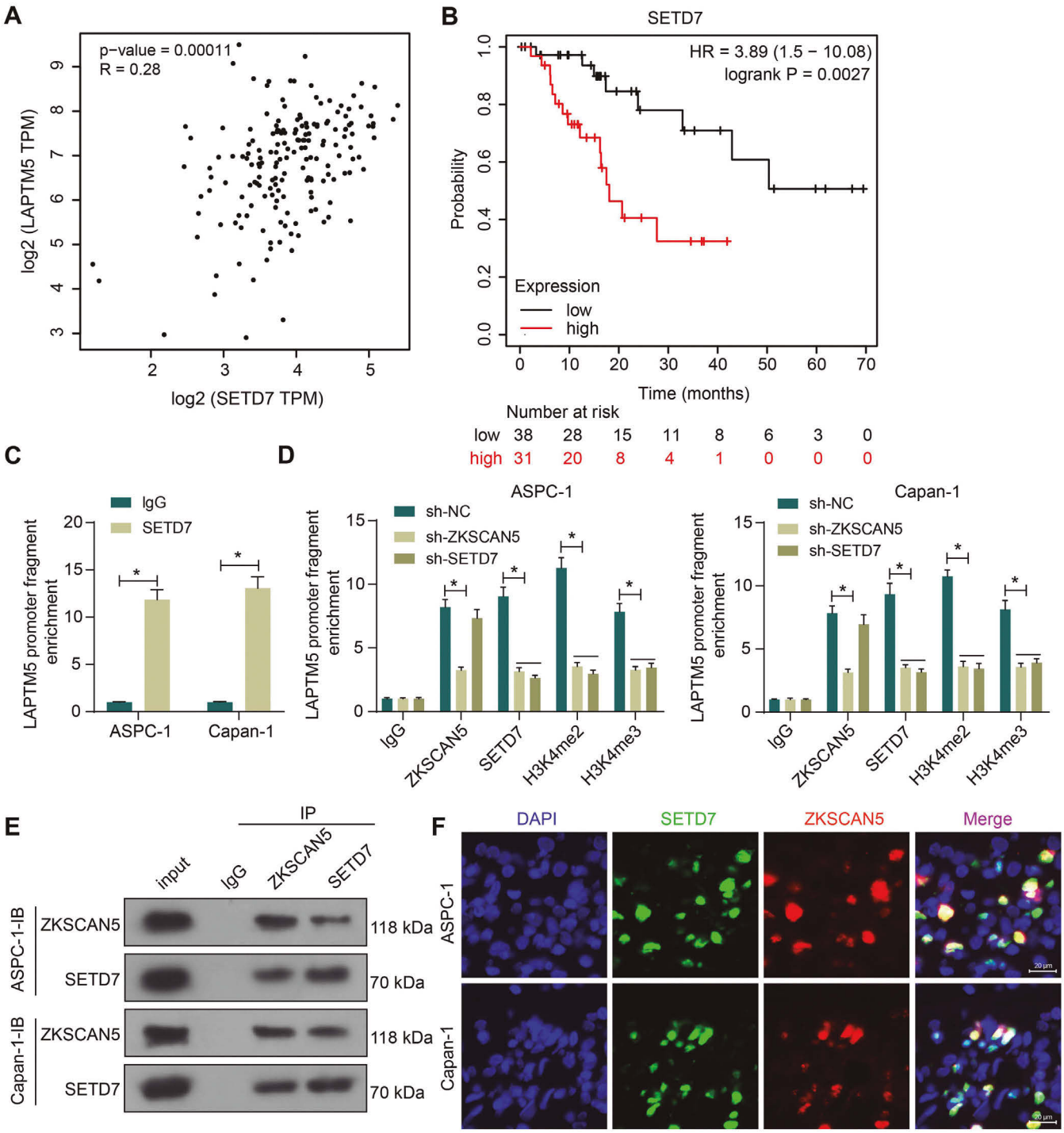

Fig. 5. ZKSCAN5 recruits SETD7. **A.** GEPIA analysis of the correlation between LAPTM5 and SETD7 expression in tumor tissues of pancreatic adenocarcinoma patients (from RNA-Seq data of TCGA-pancreatic adenocarcinoma). **B.** The prognostic value of SETD7 in predicting RFS of PDAC patients in Kaplan-Meier Plotter (n=177, RNA-seq HTSeq counts and survival data were acquired from the TCGA-PDAC repository). **C.** The enrichment of SETD7 on the LAPTM5 promoter in ASPC-1 and Capan-1 cells using ChIP-qPCR assay. **D.** The effect of knockdown of ZKSCAN5 or SETD7 on the levels of SETD7, ZKSCAN5, H3K4me2, and H3K4me3 bound to the LAPTM5 promoter in ASPC-1 and Capan-1 cells using ChIP-qPCR assay. **E.** The interaction between ZKSCAN5 and SETD7 was analyzed using Co-IP. **F.** The co-localization of ZKSCAN5 and SETD7 in PDAC cells using immunofluorescence staining. Data are presented as the mean ± S.D. n=3. *p<0.05 by two-way ANOVA.

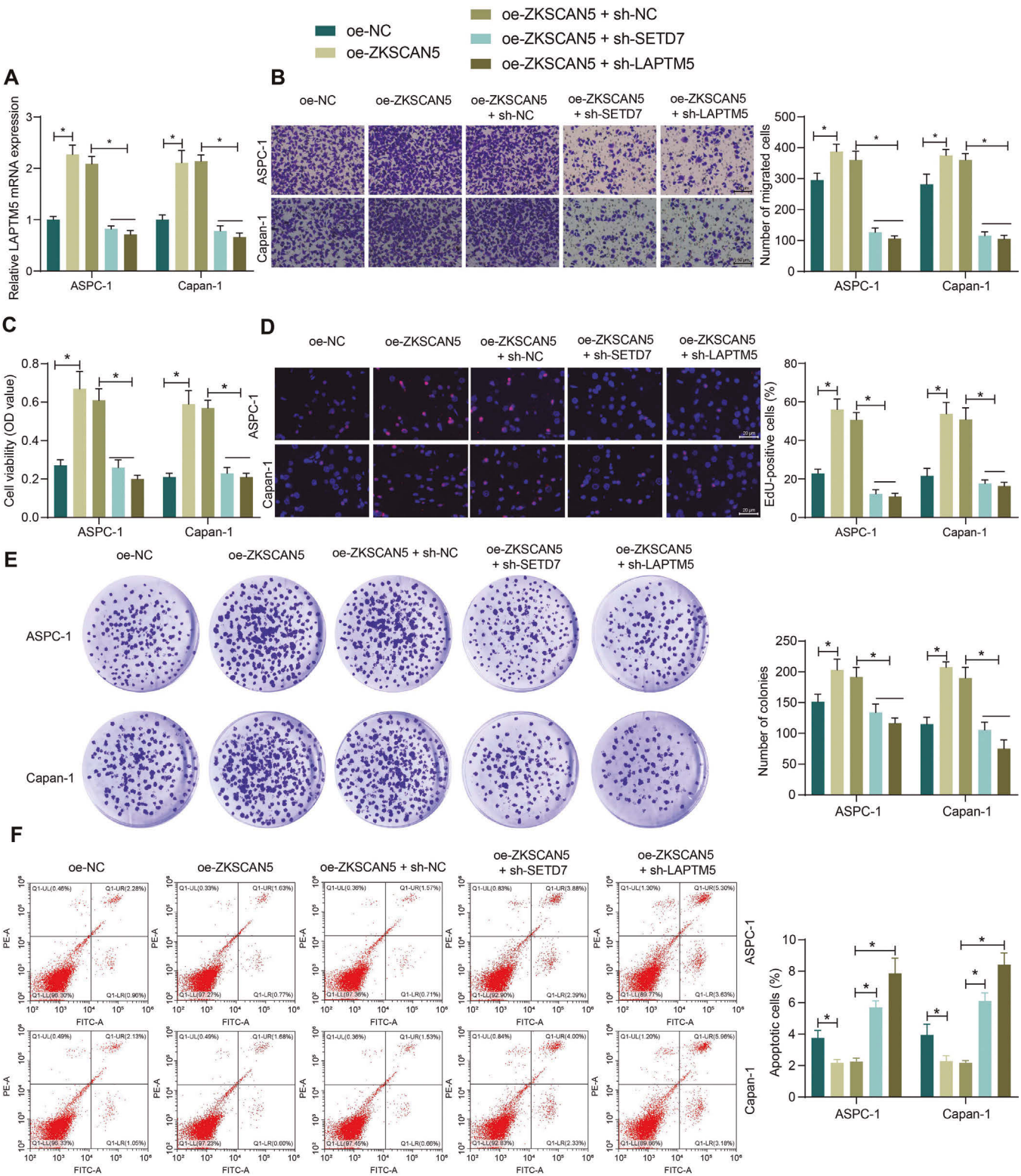

Fig. 6. ZKSCAN5 recruits SETD7 to form a transcriptional complex in PDAC. PDAC cells were infected with oe-ZKSCAN5 (oe-NC as control) or in combination with sh-SETD7 or sh-LAPTM5 (oe-ZKSCAN5 + sh-NC as control). **A.** LAPTM5 mRNA expression in ASPC-1 and Capan-1 cells after infection by RT-qPCR. **B.** ASPC-1 and Capan-1 cell migration ability by Transwell migration assay. **C.** ASPC-1 and Capan-1 cell viability by the CCK-8 assay. **D.** The proliferation ability of ASPC-1 and Capan-1 cells by the EdU incorporation assay. **E.** The colony formation ability of ASPC-1 and Capan-1 cells by colony formation assay. **F.** Apoptosis levels in ASPC-1 and Capan-1 cells by flow cytometry. Data are presented as the mean ± S.D. n=3. *$p<0.05$ by two-way ANOVA.

ZKSCAN5 in pancreatic adenocarcinoma (Fig. 4B), and Kaplan-Meier Plotter analysis predicted that patients with higher ZKSCAN5 expression had a lower RFS (Fig. 4C). ChIP-qPCR analysis demonstrated that ZKSCAN5 significantly pulled down the promoter fragment of LAPTM5 (Fig. 4D). According to the dual-luciferase reporter assay, the knockdown of ZKSCAN5 resulted in a significant decrease in the luciferase activity of luciferase reporter vectors containing the LAPTM5 promoter fragment (Fig. 4E). RT-qPCR detection of LAPTM5 mRNA expression showed that the expression of LAPTM5 was much lower after the knockdown of ZKSCAN5 (Fig. 4F). The above results confirm that ZKSCAN5 regulates the transcriptional activity of the LAPTM5 promoter to influence its transcription.

ZKSCAN5 recruits SETD7 to the promoter of LAPTM5

The expression of LAPTM5 in PDAC was significantly and positively correlated with SETD7 in GEPIA (Fig. 5A), while Kaplan-Meier Plotter analysis showed that PDAC patients with higher SETD7 expression had lower RFS (Fig. 5B). We therefore hypothesized that ZKSCAN5 mediated the transcriptional activation of LAPTM5 through the recruitment of SETD7. ChIP-qPCR experiments showed that SETD7 was also bound to the LAPTM5 promoter (Fig. 5C). By knocking down the expression of ZKSCAN5, the binding of ZKSCAN5 to the LAPTM5 promoter was significantly reduced. This also resulted in decreased levels of histone methylation on the LAPTM5 promoter, as evidenced by reduced LAPTM5 promoter fragments pulled down by antibodies to SETD7, H3K4me2, and H3K4me3. This is similar to the reduction in histone methylation levels caused by the knockdown of SETD7 alone, and the knockdown of SETD7 alone did not affect ZKSCAN5 binding to the LAPTM5 promoter (Fig. 5D), which proves that SETD7 is recruited by ZKSCAN5 that binds to the LAPTM5 promoter, rather than SETD7 that recruits ZKSCAN5. The interaction between ZKSCAN5 and SETD7 was studied by Co-IP, and the results showed that SETD7 can interact with ZKSCAN5 to form a complex in PDAC cells (Fig. 5E). We further detected the subcellular localization of both proteins using immunofluorescence, and the results suggested that both ZKSCAN5 and SETD7 were mainly distributed in the nuclei of PDAC cells (Fig. 5F).

ZKSCAN5 recruits SETD7 to form a transcriptional complex to promote the metastasis of PDAC cells

We infected ASPC-1 and Capan-1 cells overexpressing ZKSCAN5 with lentivirus harboring sh-SETD7 or sh-LAPTM5, respectively. RT-qPCR experiments showed that overexpression of ZKSCAN5 significantly increased LAPTM5 expression, and knockdown of SETD7 or LAPTM5 also significantly decreased LAPTM5 expression (Fig. 6A). Transwell migration assays showed that the migration of PDAC cells overexpressing ZKSCAN5 was potentiated, which was inhibited after the knockdown of SETD7 or LAPTM5 (Fig. 6B). CCK-8 and EdU incorporation assays showed that ectopic expression of ZKSCAN5 significantly promoted the viability and proliferation of PDAC cells, and knockdown of SETD7 or LAPTM5 repressed the viability and proliferation of PDAC cells (Fig. 6C,D). Colony formation assay revealed increased colony formation in cells overexpressing ZKSCAN5 and decreased colony formation in cells with SETD7 or LAPTM5 knockdown (Fig. 6E). Finally, the anti-apoptotic effects of ZKSCAN5 on PDAC cells were reversed by SETD7 and LAPTM5 knockdown (Fig. 6F).

Discussion

Pancreatic cancer remains a fatal disease with a five-year survival rate of about 10% in the USA as approximately 80-85% of patients have either unresectable or metastatic diseases (Mizrahi et al., 2020). Therefore, understanding the molecular mechanism underlying the metastatic process is a mainstream focus of PDAC research. The present study demonstrated that inhibition of LAPTM5 by shRNA reduced the neoplastic features, such as cell viability, proliferation, colony formation, and migratory potential in PDAC cell lines, and prevented metastatic dissemination into the liver. Molecular investigations revealed that the transcription of LAPTM5 was regulated by the ZKSCAN5 recruitment of SETD7.

According to a Kaplan-Meier survival analysis of renal clear cell carcinoma datasets, a LAPTM5 low-expression cohort had a 118.47-month survival, while the high-expression cohort had a 73.00-month survival (p=0.0088) (Fang and Wang, 2022). Functionally, LAPTM5 maintained the self-renewal and cancer stem cell-like properties of renal cancer cells by repressing the function of lung-derived bone morphogenetic proteins (Jiang et al., 2022). Furthermore, loss of LAPTM5 hampered proliferation and viability and stimulated G0/G1 cell cycle arrest of bladder cancer cells (Chen et al., 2017). In the present study, we substantiated the promotion of LAPTM5 expression in metastatic PDAC cells (ASPC-1, CFPAC-1, and Capan-1) relative to BxPC-3 cells. In addition, the *in vitro* and *in vivo* evidence revealed that loss of LAPTM5 restricted the malignant traits of metastatic ASPC-1 and Capan-1 cells, including cell viability, proliferation, colony formation, tube formation, and apoptosis resistance. Consistently, the inhibitory effects of long noncoding RNA LCDR and heterogenous nuclear ribonucleoprotein K knockdown on xenograft tumor growth and mass of NCI-H1299 cells were partially rescued by LAPTM5 overexpression (Yang et al., 2022). Here, we observed the reduced number of liver nodules formed by the ASPC-1 cells infected with sh-LAPTM5. LAPTM5 was also related to $CD8^+$ T cell and PDCD1 expression in testicular germ cell tumors, which suggests its implication in immune

infiltration (Li et al., 2021). Given the fact that the establishment of the pre-metastatic niche is encouraged by neutrophils and hematopoietic immune progenitor cells and inflammatory cytokines released from these immune cells (Smith and Kang, 2013), the role of LAPTM5 in mediating immune infiltration awaits further exploration.

To better understand the mechanism of action of LAPTM5 in PDAC, we queried the bioinformatics website and identified the physical binding site between LAPTM5 and ZKSCAN5. Due to their complex regulation, ZKSCAN transcription factors have been demonstrated to possess promotive or prohibitive efforts in angiogenesis, cell apoptosis, proliferation, and stem cell properties (Huang et al., 2019). More compelling, ZKSCAN5 has been implicated in the immuno-surveillance and distant metastases in colorectal cancer (Jacob et al., 2021). The promoter methylation levels of LAPTM5 in clear cell renal cell carcinoma tissues were significantly lower than those in normal tissues (Sui et al., 2021), indicating that the dysregulation of LAPTM5 was associated with methylation. Across eukaryotic genomes, lysine methylation at H3K4 is usually related to transcriptional activation (Keating and El-Osta, 2013). For instance, GATA1, a transcription factor, enhanced breast cancer cell-secreted vascular endothelial growth factor via SETD7-mediated H3K4 methylation, which promoted HUVEC proliferation, migration, and tube formation (Zhang et al., 2016). SETD7 is a 41-kDa lysine mono-methyltransferase that regulates the methylation of different histone and non-histone substrates (Batista and Helguero, 2018). SET7-mediated UHRF1 methylation is essential for cell viability against DNA damage (Hahm et al., 2019). Similarly, we observed that the knockdown of ZKSCAN5 led to reduced occupancy of SETD7, H3K4me2, and H3K4me3 on the LAPTM5 promoter, indicating that ZKSCAN5 recruited SETD7 to the promoter region of LAPTM5, thereby manipulating the transcription of LAPTM5. Fujimaki et al., reported that SETD7/9 contributed to Nos2 transcription in pancreatic β cells through activating histone modifications (Fujimaki et al., 2015). The most studied processes regulated by SETD7 in cancers were cell proliferation, apoptosis, EMT, migration, and invasion (Monteiro et al., 2022). Our rescue experiments using shRNAs targeting LAPTM5 and SETD7 on PDAC cells overexpressing ZKSCAN5 showed that knockdown of downstream LAPTM5 and SETD7 suppressed the oncogenic effects of ZKSCAN5. The positive effects of SETD7 on cell proliferation, migration, and invasion were also reported in breast cancer cells (Si et al., 2020).

Conclusion

To summarize, we discovered the metastasis-promoting properties of LAPTM5 whose transcription was governed by ZKSCAN5 recruitment of SETD7 in PDAC. In this study, we suggest a novel mechanism of liver metastasis in PDAC through the exquisite modulation of LAPTM5's methylation status by SETD7 and ZKSCAN5.

Funding. None.

Conflict of interest. The authors declare that they have no competing interests.

Data availability statement. All data generated or analyzed during this study are included in this published article.

Author Contributions. YY was responsible for the design of the study, data analysis, and manuscript writing; WX contributed to data acquisition, analysis, and interpretation, and also drafted and critically revised the manuscript; XQ and JY contributed to the analysis and interpretation of the data; DY and DMZ contributed to the data collection, statistical analysis, and manuscript review. All authors read and approved the final manuscript.

References

Batista I.A.A. and Helguero L.A. (2018). Biological processes and signal transduction pathways regulated by the protein methyltransferase SETD7 and their significance in cancer. Signal Transduct. Target. Ther. 3, 19.

Chen L., Wang G., Luo Y., Wang Y., Xie C., Jiang W., Xiao Y., Qian G. and Wang X. (2017). Downregulation of LAPTM5 suppresses cell proliferation and viability inducing cell cycle arrest at G0/G1 phase of bladder cancer cells. Int. J. Oncol. 50, 263-271.

Chiang C., Yang H., Zhu L., Chen C., Chen C., Zuo Y. and Zheng D. (2022). The epigenetic regulation of nonhistone proteins by SETD7: New targets in cancer. Front. Genet. 13, 918509.

De Dosso S., Siebenhuner A.R., Winder T., Meisel A., Fritsch R., Astaras C., Szturz P. and Borner M. (2021). Treatment landscape of metastatic pancreatic cancer. Cancer Treat. Rev. 96, 102180.

Fahr L., Sunami Y., Maeritz N., Steiger K., Grunewald T.G.P., Gericke M., Kong B., Raulefs S., Mayerle J., Michalski C.W., Regel I. and Kleeff J. (2020). Expression of the EWSR1-FLI1 fusion oncogene in pancreas cells drives pancreatic atrophy and lipomatosis. Pancreatology 20, 1673-1681.

Fang G. and Wang X. (2022). Prognosis-related genes participate in immunotherapy of renal clear cell carcinoma possibly by targeting dendritic cells. Front. Cell Dev. Biol. 10, 892616.

Fujimaki K., Ogihara T., Morris D.L., Oda H., Iida H., Fujitani Y., Mirmira R.G., Evans-Molina C. and Watada H. (2015). SET7/9 enzyme regulates cytokine-induced expression of inducible nitric-oxide synthase through methylation of lysine 4 at histone 3 in the islet β cell. J. Biol. Chem. 290, 16607-16618.

Gasmi A., Peana M., Arshad M., Butnariu M., Menzel A. and Bjorklund G. (2021). Krebs cycle: Activators, inhibitors and their roles in the modulation of carcinogenesis. Arch. Toxicol. 95, 1161-1178.

Geng Y.M., Liu C.X., Lu W.Y., Liu P., Yuan P.Y., Liu W.L., Xu P.P. and Shen X.Q. (2019). LAPTM5 is transactivated by RUNX2 and involved in RANKL trafficking in osteoblastic cells. Mol. Med. Rep. 20, 4193-4201.

Hahm J.Y., Kim J.Y., Park J.W., Kang J.Y., Kim K.B., Kim S.R., Cho H. and Seo S.B. (2019). Methylation of UHRF1 by SET7 is essential for DNA double-strand break repair. Nucleic Acids Res. 47, 184-196.

Huang M., Chen Y., Han D., Lei Z. and Chu X. (2019). Role of the zinc finger and SCAN domain-containing transcription factors in cancer.

Am. J. Cancer Res. 9, 816-836.

Jacob S., Jurinovic V., Lampert C., Pretzsch E., Kumbrink J., Neumann J., Haoyu R., Renz B.W., Kirchner T., Guba M.O., Werner J., Angele M.K. and Bosch F. (2021). The association of immunosurveillance and distant metastases in colorectal cancer. J. Cancer Res. Clin. Oncol. 147, 3333-3341.

Jiang B., Zhao X., Chen W., Diao W., Ding M., Qin H., Li B., Cao W., Chen W., Fu Y., He K., Gao J., Chen M., Lin T., Deng Y., Yan C. and Guo H. (2022). Lysosomal protein transmembrane 5 promotes lung-specific metastasis by regulating BMPR1A lysosomal degradation. Nat. Commun. 13, 4141.

Keating S.T. and El-Osta A. (2013). Transcriptional regulation by the Set7 lysine methyltransferase. Epigenetics 8, 361-372.

Li X., Su Y., Zhang J., Zhu Y., Xu Y. and Wu G. (2021). LAPTM5 plays a key role in the diagnosis and prognosis of testicular germ cell tumors. Int. J. Genomics 2021, 8816456.

Li J., Yan Z., Ma J., Chu Z., Li H., Guo J., Zhang Q., Zhao H., Li Y. and Wang T. (2022). ZKSCAN5 activates VEGFC expression by recruiting SETD7 to promote the lymphangiogenesis, tumour growth, and metastasis of breast cancer. Front. Oncol. 12, 875033.

Mizrahi J.D., Surana R., Valle J.W. and Shroff R.T. (2020). Pancreatic cancer. Lancet 395, 2008-2020.

Monteiro F.L., Williams C. and Helguero L.A. (2022). A systematic review to define the multi-faceted role of lysine methyltransferase SETD7 in cancer. Cancers (Basel) 14, 1414.

Nakata K., Ohuchida K., Nagai E., Hayashi A., Miyasaka Y., Kayashima T., Yu J., Aishima S., Oda Y., Mizumoto K., Tanaka M. and Tsuneyoshi M. (2009). LMO2 is a novel predictive marker for a better prognosis in pancreatic cancer. Neoplasia 11, 712-719.

Ouyang H., Wang P., Meng Z., Chen Z., Yu E., Jin H., Chang D.Z., Liao Z., Cohen L. and Liu L. (2011). Multimodality treatment of pancreatic cancer with liver metastases using chemotherapy, radiation therapy, and/or chinese herbal medicine. Pancreas 40, 120-125.

Ren B., Cui M., Yang G., Wang H., Feng M., You L. and Zhao Y. (2018). Tumor microenvironment participates in metastasis of pancreatic cancer. Mol. Cancer 17, 108.

Si W., Zhou J., Zhao Y., Zheng J. and Cui L. (2020). SET7/9 promotes multiple malignant processes in breast cancer development via RUNX2 activation and is negatively regulated by TRIM21. Cell Death Dis. 11, 151.

Smith H.A. and Kang Y. (2013). The metastasis-promoting roles of tumor-associated immune cells. J. Mol. Med. (Berl) 91, 411-429.

Sui Y., Lu K. and Fu L. (2021). Prediction and analysis of novel key genes ITGAX, LAPTM5, SERPINE1 in clear cell renal cell carcinoma through bioinformatics analysis. PeerJ 9, e11272.

Tsilimigras D.I., Brodt P., Clavien P.A., Muschel R.J., D'Angelica M.I., Endo I., Parks R.W., Doyle M., de Santibanes E. and Pawlik T.M. (2021). Liver metastases. Nat. Rev. Dis. Primers 7, 27.

Viloria K., Munasinghe A., Asher S., Bogyere R., Jones L. and Hill N.J. (2016). A holistic approach to dissecting SPARC family protein complexity reveals FSTL-1 as an inhibitor of pancreatic cancer cell growth. Sci. Rep. 6, 37839.

Yang X., Wen Y., Liu S., Duan L., Liu T., Tong Z., Wang Z., Gu Y., Xi Y., Wang X., Luo D., Zhang R., Liu Y., Wang Y., Cheng T., Jiang S., Zhu X., Yang X., Pan Y., Cheng S., Ye Q., Chen J., Xu X. and Gao S. (2022). LCDR regulates the integrity of lysosomal membrane by hnRNP K-stabilized LAPTM5 transcript and promotes cell survival. Proc. Natl. Acad. Sci. USA 119, e2110428119.

Zafar S., Armaghan M., Khan K., Hassan N., Sharifi-Rad J., Habtemariam S., Kieliszek M., Butnariu M., Bagiu I.C., Bagiu R.V. and Cho W.C. (2023). New insights into the anticancer therapeutic potential of maytansine and its derivatives. Biomed. Pharmacother. 165, 115039.

Zhang Y., Liu J., Lin J., Zhou L., Song Y., Wei B., Luo X., Chen Z., Chen Y., Xiong J., Xu X., Ding L. and Ye Q. (2016). The transcription factor GATA1 and the histone methyltransferase SET7 interact to promote VEGF-mediated angiogenesis and tumor growth and predict clinical outcome of breast cancer. Oncotarget 7, 9859-9875.

Accepted November 22, 2023